 FDMP, vol.14, no.1, pp.1-21, 2018

Numerical Study of Natural Convection in a Right Triangular Enclosure with Sinusoidal Hot Wall and Different Configurations of Cold Walls

Manoj Kr. Triveni[1, *] and Rajsekhar Panua[2]

Abstract: The numerical investigation of present work examines the free convection cooling of the base hot wall of a right-angled triangular cavity filled with water. The outline of the base wall is changed from smooth to sinusoidal shapes with different heights. The width (w) of the wave is fixed at 0.2 L and the height (h) of the sinusoidal shape wall is varied from 0.01 H to 0.03 H. The hot wall is cooled from the partially active side and inclined walls which are detached from the middle and structured in four different configurations namely AB, BC, AD, and CD. The problem has been solved to explore the effect of constrained parameters such as a sinusoidal hot wall, partially active cold walls' configurations and Rayleigh number (10^5-10^7) on fluid flow and heat transfer. The study reveals that the flow pattern of the fluid is affected due to the configurations of cold walls and with the increase of Rayleigh number. The enhancement in heat transfer rate, in fact, is found to be more pronounced for the amalgamation of the sinusoidal hot wall and the cold walls configuration AB for all Rayleigh number. However, the blends of these are appealing eloquently at low Rayleigh number.

Keywords: Sinusoidal hot wall, cold walls configurations, triangular cavity, Rayleigh number, Natural convection.

Nomenclature

g	acceleration due to gravity
H	height of the cavity
b	width of the cavity
s	hypotenuse of the cavity
h	height of the C-curve
w	width of the curve
δ	aspect ratio of the curve (h/s)
p	pressure
P	dimensionless pressure
u, v	velocity components
T_c	cold wall temperature
Pr	Prandtl number
Ra	Rayleigh number

Greek symbols

α	thermal diffusivity
β	thermal expansion coefficient
θ	dimensionless temperature
k	thermal conductivity
ρ	density
μ	dynamic viscosity

[1] Department of Mechanical Engineering, the ICFAI University, Agartala, Tripura, 799210.

[2] Department of Mechanical Engineering, National Institute of Technology, Agartala, Tripura, 799046.

* Corresponding author: Manoj Kr. Triveni. Email: triveni_mikky@yahoo.com.

U, V dimensionless velocity components
x, y co-ordinates system
X, Y dimensionless co-ordinates system
T temperature
T_h hot wall temperature
Nu_x local Nusselt number
Nu average Nusselt number
υ kinematic viscosity
ψ stream function
Ψ dimensionless stream function

Subscripts

h hot wall
c cold wall
FLC full length of cold walls

1 Introduction

The fluid flow behavior and heat transfer characteristics through natural convection within enclosures filled with fluid are well established [Flack, Konopnicki and Rooke (1979); Nansteel (1984); Ostrach (1988); Ganzarolli and Milanez (1995)]. Even though the cooling efficiency via free convection is less compared to that of forced convection still it has drawn the researchers' attention significantly. Buoyancy-induced flow makes the natural convection economical and is being widely used in various applications such as solar energy system, electronics equipment, and many other applications. Numerous works have been done through experimental, numerical in different enclosures; square, rectangular, rhombic, triangular etc. [Pesso and Piva (2009); Bocu and Altac (2011); Triveni, Sen and Panua (2014); Ramakrishn, Basak, Roy et al. (2014); Nasr, Chouikh, Kerkeni et al. (2006); Triveni and Panua (2016)] to examine the heat transfer rate. But, plenty of works are yet in progress to improve the cooling rate from the enclosures.

In this modern era, the uses of nanoparticles with different types of fluids inside enclosures have been widely accepted and significantly used to enhance the cooling efficiency. Rahimi et al. [Rahimi, Ranjbar and Hosseini (2012)] have numerically studied the natural convection in a rectangular enclosure using Cu nanoparticles based nanofluid. It was reported that the density inversion and nanoparticles with more than 5% of the volume fraction are led to reducing the heat transfer rate. Abu-Nada et al. [Abu-Nada, Masoud, Oztop et al. (2010)] examined the heat transfer by free convection in a square enclosure employing different types of nanofluids. They concluded that the nanoparticles with less than 5% of volume fraction and enclosure with low aspect ratio have performed better for heat transfer rate enhancement. Aminossadati [Aminossadati (2013)] worked on natural convection in a CuO-water based nanofluid filled right triangular enclosure. They found that the overall heat transfer rate was decreased as the heat source moved away from the cold walls for all Rayleigh number. However, the CuO-water based nanofluid enhanced the thermal performance of the cavity at lower Rayleigh number.

Nevertheless, many studies reported that the nanoparticles are effective at low volume fraction and also the heat transfer rate is enhanced by 10 to 20% [Aminossadati (2013)]. But, the adoption of nanoparticles may increase the cost of cooling which may not be more economical. It is also very well-known that the heat transfer rate is more pronounced for irregular surface structure than the smooth surface. Hence, heating or cooling of the cavity using irregular surface may be well economical and more effective if the heat transfer rate is more pronounced than the use of nanofluids. Since electronic

components size may not always be identical. Subsequently, cooling of equipment with lesser heat transfer by using smooth wall may not justify the system design. Thus, the irregular surface model which may enhance the cooling rate of the cavity by natural convection may be applicable for system design. Also, triangular enclosures heating from the side or below are substantially employed in the domestics and industrial applications [Akinsete and Coleman (1982); Triveni, Panua and Sen (2015); Asan and Namli (2000); Triveni and Panua (2016)]. A few studies have been done with the convective heat transfer within enclosures using complex surfaces. Dalal et al. [Dalal and Das (2005)] investigated the natural convection in a square cavity using the wavy wall on the right side, numerically. They found that the average Nusselt number was increased at low Rayleigh number while decreased with the increase in Rayleigh number. A numerical work is carried out by Rahman et al. [Rahman, Oztop, Ahsan et al. (2012)] to study the effect of Buoyancy ratio (Br) and Lewis number (Le) on the heat and mass transfer in a triangular cavity with zig-zag shaped bottom wall. It was reported that the average Nusselt and Sherwood numbers have been increased by 89.18% and 101.91% respectively as Br was increased from 10 to 20. While the average Nusselt has been decreased by 16.22% and Sherwood number has been increased by 144.84% as Le is increased from 0.1 to 20. Rahman et al. [Rahman, Saidur, Mekhilef et al. (2013)] have studied the heat transfer in a corrugated base surface triangular enclosure numerically. Results revealed that both heat and mass transfer were enhanced with the increase of the wavelength and Rayleigh number.

From the above survey, it is worthy to state that the majority of the studies have been taken into consideration for improving the rate of heat transfer of the cavity by natural convection via numerous methods and processes. The present work also takes part in the process of heat transfer enhancement by modifying the geometry of the triangular cavity. Hence, the prime objective of this study is to examine the cooling rate by laminar natural convection from the right triangular cavity using a sinusoidal hot wall with partially active cold walls.

2 Physical model description and mathematical formulation

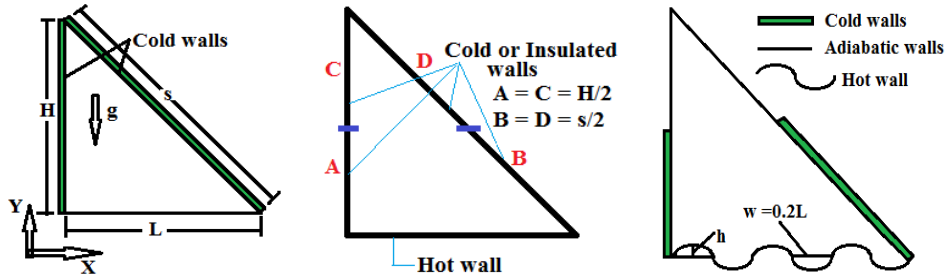

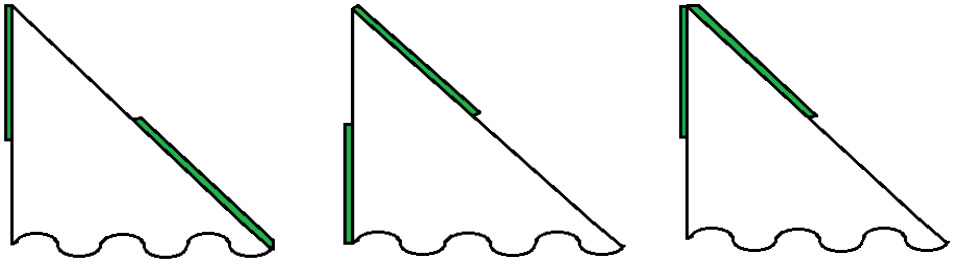

Figure 1: Schematic diagrams of physical model with constrained boundary conditions

Fig. 1 shows the physical model of 2-D isosceles right-angled triangular enclosure associated with constrained boundary conditions. The width of the cavity is L and height H. The cavity base wall is integrated with one smooth and three different heights of sinusoidal walls. The width (w) of the sinusoidal is fixed at 0.2 L while the height (h) of the waves is varied from 0.25 H to 0.75 H. The aspect ratio (δ=h/w) of the curve is changed from 0.05 to 0.15. While, at n=0, the wall is treated as a smooth wall. The cavity's side and hypotenuse wall are detached from the middle, A=C=H/2 & B=D=s/2, arranged into four different configurations AB, BC, AD, and CD and made it partially active. It has been made sure that only one configuration is active at a time, however, remaining parts are kept adiabatic. The base wall of the enclosure is considered as a hot wall which maintained at constant temperature T_h while the cold walls' temperature is maintained at steady temperature T_c (T_h>T_c). Copper is implemented for the thermally active part while an insulating material Plexiglas has been used for adiabatic walls.

The cavity is filled with water and flow is assumed to be incompressible. Some assumptions have been made such as; all walls of the enclosure are impermeable, viscous effect of the working fluid and radiation heat transfer are neglected and all fluid properties are presumed to be constant except density variation in y-momentum which is changed with temperature, to formulate the continuity, momentum and energy equations for steady-state laminar flow inside a triangular cavity. Based on the above suppositions and using the dimensionless parameters, the non-dimensional governing equations with negligible viscous dissipation are written as:

$$X = \frac{x}{H}, Y = \frac{y}{H}, U = \frac{uH}{\alpha}, V = \frac{vH}{\alpha}, \theta = \frac{T-T_c}{T_h-T_c}, P = \frac{pH^2}{\rho\alpha^2}, Pr = \frac{\vartheta}{\alpha}, Ra = \frac{g\beta(T_h-T_c)H^3}{\alpha\vartheta} \quad (1)$$

$$\frac{\partial U}{\partial X} + \frac{\partial V}{\partial Y} = 0 \quad (2)$$

$$U\frac{\partial U}{\partial X} + V\frac{\partial U}{\partial Y} = -\frac{\partial P}{\partial X} + \Pr\left(\frac{\partial^2 U}{\partial X^2} + \frac{\partial^2 U}{\partial Y^2}\right) \quad (3)$$

$$U\frac{\partial V}{\partial X} + V\frac{\partial V}{\partial Y} = -\frac{\partial P}{\partial Y} + \Pr\left(\frac{\partial^2 V}{\partial X^2} + \frac{\partial^2 V}{\partial Y^2}\right) + RaPr\theta \quad (4)$$

$$U\frac{\partial \theta}{\partial X} + V\frac{\partial \theta}{\partial Y} = \left(\frac{\partial^2 \theta}{\partial X^2} + \frac{\partial^2 \theta}{\partial Y^2}\right) \quad (5)$$

Dimensionless boundary conditions of the cavity

Table 1: For both side (vertical and inclined) cooling

Hot wall	**Cold Wall**	**Adiabatic Wall**
θ=1, U=V=0 at Y=0 at 0≤ X ≤ 1	Vertical cold wall: θ=0, U=V=0 at X=0 and 0<Y<1 Inclined cold wall: θ=0, U=V=0 at 0 < X < 1 and 0 < Y < 1	
	For partial cooling	
θ=1, U=V=0 at Y=0 at 0≤X≤1	Lower half of the side wall: θ=0, U=V=0 at X=0, 0≤Y≤1/2	Upper half of the side wall: ∂θ/∂n=0, U=V=0 at X=0, 1/2≤Y≤1
	Upper half of the side wall: θ=0, U=V=0 at X=0, 1/2≤Y≤1	Lower half of the side wall: ∂θ/∂n=0, U=V=0 at X=0, 0≤Y≤1/2
	Lower half of the hypotenuse wall: θ=0, U=V=0 at 1/2≤X≤1 and 0≤Y≤1/2	Upper half of the hypotenuse wall: ∂θ/∂n=0, U=V=0 at 0≤X≤1/2 and 1/2 ≤ Y≤ 1
	Upper half of the hypotenuse wall: θ=0, U=V=0 at 0≤X≤1/2 and 1/2≤Y≤1	Lower half of the hypotenuse wall: ∂θ/∂n=0, U=V=0 at 1/2≤X≤ 1 and 0≤Y≤1/2

3 Numerical procedure

A computational scheme based on finite volume method using SIMPLE algorithm is chosen, inbuilt in FLUENT 6.3 software (2005), to discretize the above presented non-dimensional governing Eqs. (2-5) along with their corresponding boundary conditions. The pressure terms are discretized by PRESTO scheme whereas the second order upwind technique is adopted for convection and diffusion terms in momentum and energy equations. The average Nusselt number is calculated by the new defined formula of Yesiloz et al. [Yesiloz and Aydin (2013)] to overcome the singularity problem in a triangular cavity which is:

$$Nu = \frac{dT}{d\emptyset}\Big|_{\emptyset=0} \frac{1}{T_h - T_c}\frac{\pi}{2} \tag{6}$$

4 Results and discussions

4.1 Numerical test and validation

Fig. 2 displays the five different uniform grid structures 60×60, 80×80, 100×100, 120×120 and 140×140 for the physical model are chosen to conduct the grid independency test. The independency on mesh structure is evaluated by the less deviation in dimensionless stream function (Ψ) and average Nusselt number (Nu). Tab. 2 presents the grid numbers influence on stream function and average Nusselt number. The relative error analysis for grids indicated that the deviation in Ψ and Nu is less than 0.5% and 1% respectively, between the mesh sizes of 120×120 and 140×140. Hence the present work is adopted 120×120 grid systems for the triangular cavity to proceed the numerical process and to obtain the excel results.

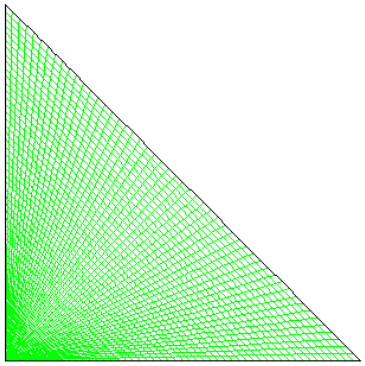

Figure 2: Recommended grid structures for present model

Table 2: Grid independency examination result

Cells	Ψ_{max}	Deviation (%)	Nu	Deviation (%)
60×60	36.04		14.95	
80×80	34.62	3.94	15.01	0.40
100×100	33.05	4.53	15.02	0.07
120×120	31.90	3.50	15.05	0.19
140×140	31.85	0.16	15.14	0.59

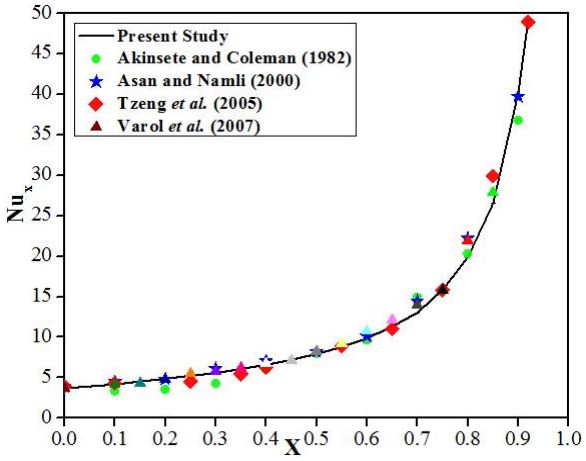

Figure 3: Assessment of the present work with other published data for triangular cavity at Ra=2772

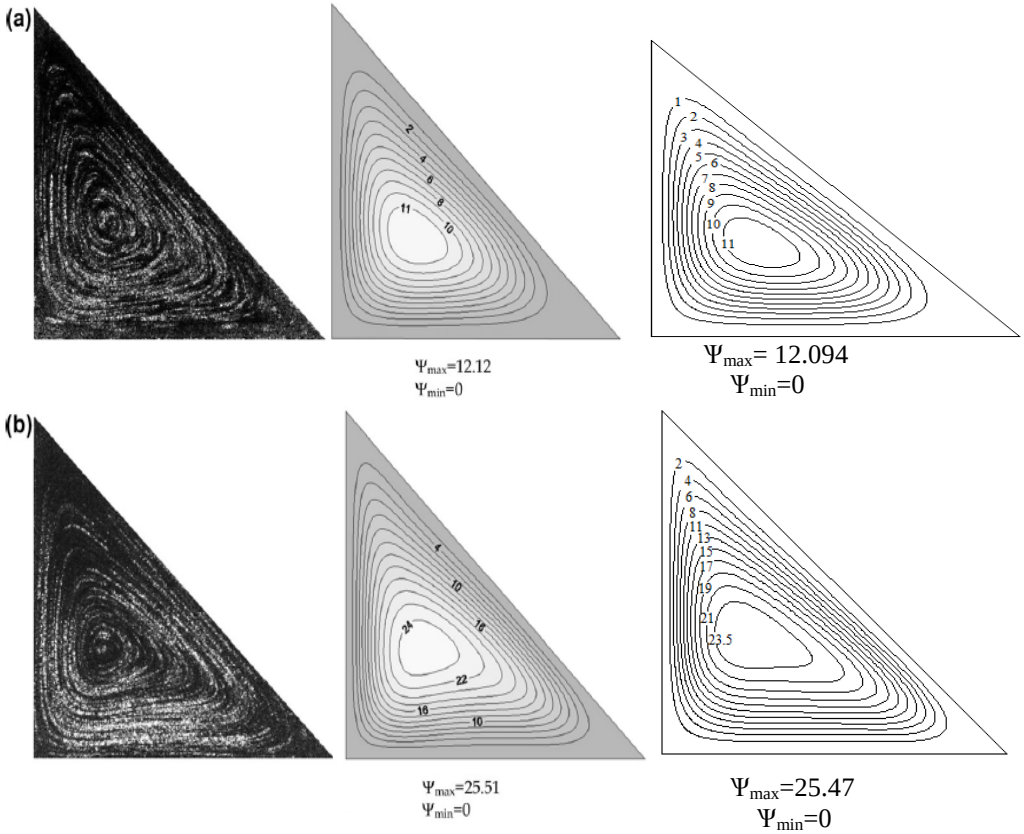

Figure 4: Experimental and numerical streamlines (left and middle) from Yesiloz and Aydin and numerical simulation (right) from the present study for a) $Ra=10^5$ and b) $Ra=5\times10^5$

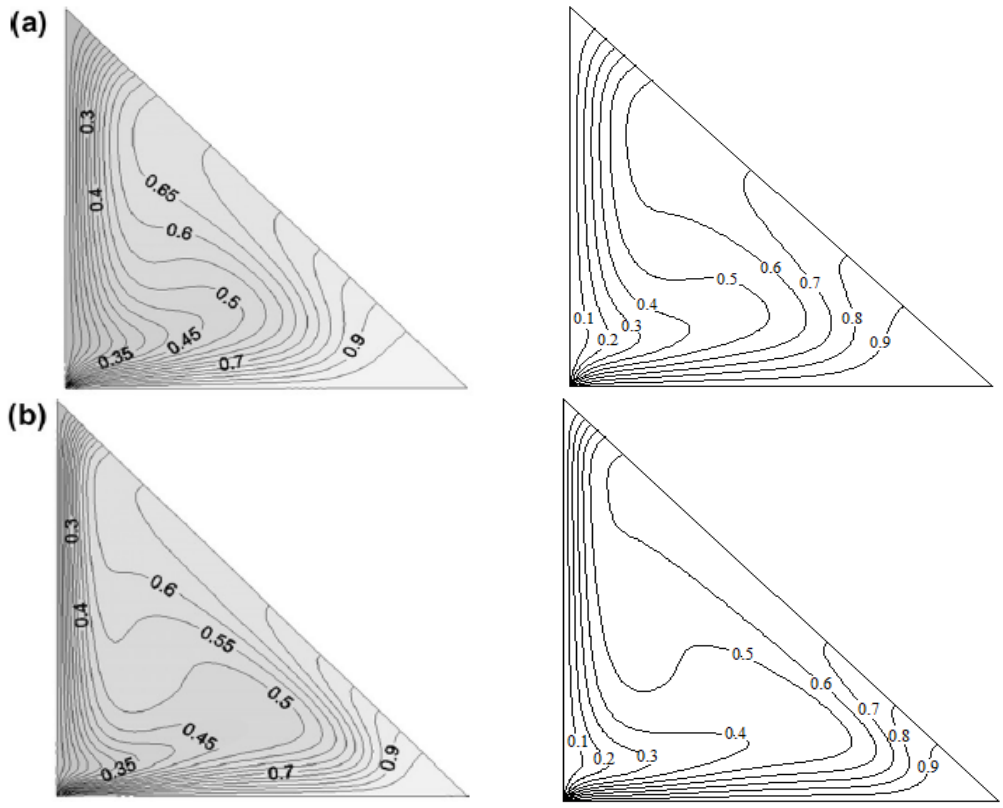

Figure 5: Experimental and numerical isotherms (left column) from Yesiloz and Aydin and numerical isotherms (right column) from the present study for a) $Ra=10^5$ and b) $Ra=5\times10^5$

The validation of the present study is carried out with the 2-D triangular enclosure filled with air with the published results, quantitatively. The work is performed for Ra=2772 and the result is validated through the local Nusselt number with the published data of Akinsete et al. [Akinsete and Coleman (1982); Asan and Namli (2000); Tzeng, Liou and Jou (2005); Varol, Oztop and Yilmaz (2007)] as shown in Fig. 3. One more study is conducted, shown in Figs. 4 and 5, in a right-angled triangular cavity filled with water, considering the same boundary conditions at $Ra=10^5$ and $Ra=5\times10^5$, to validate the results qualitatively with the existing experimental and numerical results of Yesiloz et al. [Yesiloz and Aydin (2013)]. It is quite cleared from Figs. 3-5 that the results which are validated quantitatively and qualitatively exhibited quite good agreement with the published results.

4.2 Effect of aspect ratio

δ =0

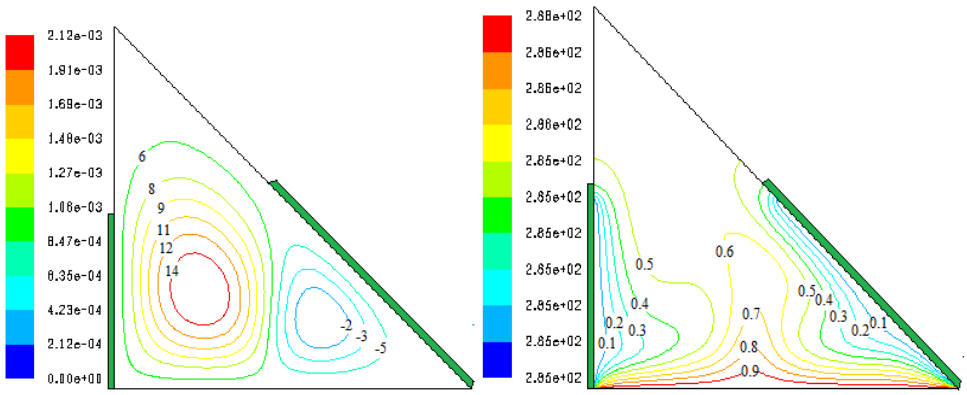

Ψ_{max}=15.18

δ = 0.05

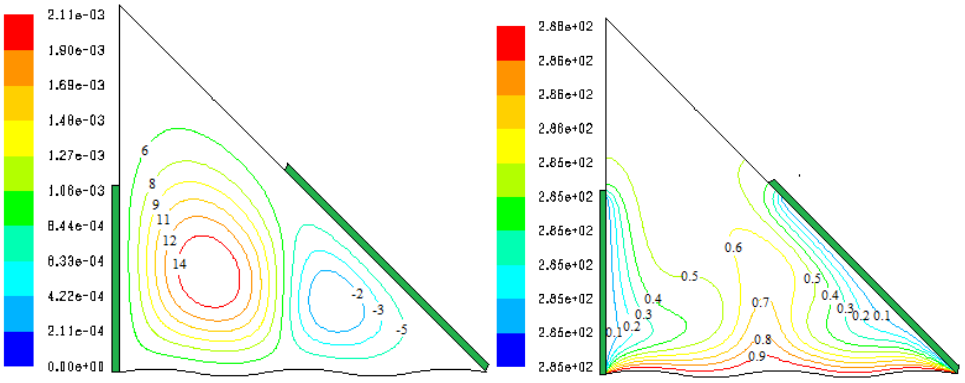

Ψ_{max}=15.13

δ = 0.1

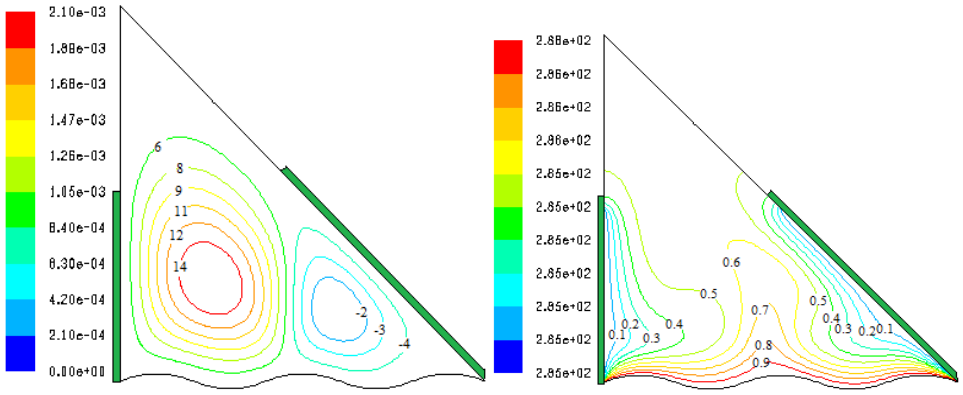

Ψ_{max}=15.1

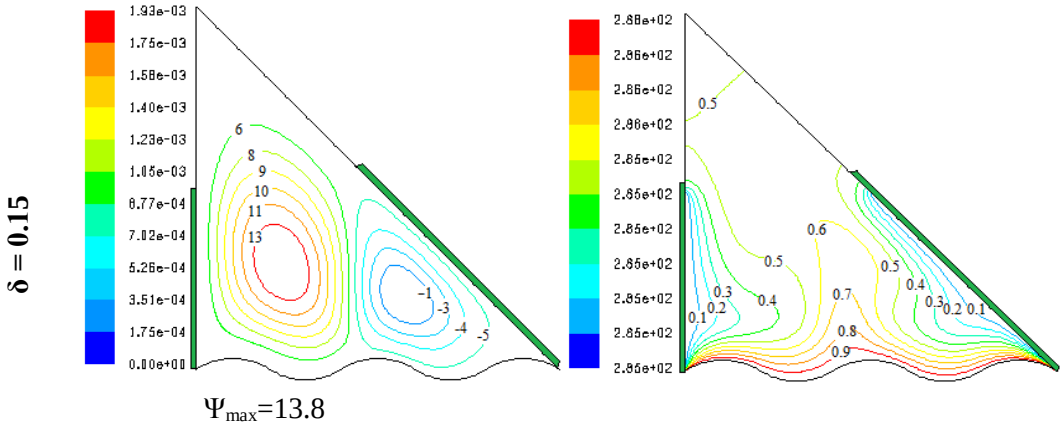

Figure 6: Variation of streamlines (left) and isotherms (right) at different *n* of the hot wall for position AB of the cold wall at Ra=10^5

Fig. 6 illustrates the streamlines (left) and isotherms (right) for different values of δ and cold walls position AB at Ra=10^5. Two asymmetric rotating cells, which have been clearly shown by streamlines, are rotated in counter directions inside the cavity for all values of δ. The bigger cell is rotated in anticlockwise and adjacent to the vertical cold wall while the smaller one in a clockwise direction nears the inclined cold wall. In the case of smooth heating, the streamlines of the larger cell are parallel in the vicinity of the hot wall. However, the shape of the streamlines is changed with the shape of the sinusoidal wall as the hot wall is changed from smooth to sinusoidal with varying the aspect ratio. The strength of the bigger cell is higher than that of the smaller cell due to its flow rotational velocity which is shown by stream function values. The positive and negative sign of the stream function values is indicated the direction of the rotation of streamlines only. It is interesting to observe that the local stream functions values are quite same for δ=0 to 0.1 and different for δ=0.15. But, the mean values of stream functions are decreased gradually with the increase of aspect ratio. Even though the rotational velocity of the fluids gets decreased, but the intensity of heat transfer is increased with the increase of δ, because the fluid particles get contacted for a longer time with the hot surface due to its sinusoidal structure.

The heat distribution inside the cavity is displayed through isotherms (right) in Fig. 6 for same boundary conditions and Rayleigh number. The emanation and end of isotherms from the base hot wall to the neighboring cold walls show the path of heat flow. The temperature contour (θ=0.9) is almost parallel to the smooth wall except at the stem of the cavity where it grows and moves upward. The value of θ is decreased as the contours move far from the hot wall which indicates the lesser exchange of heat. After θ=0.6, the isotherms are being separated and heaped near the cold walls. When the hot wall is switched from smooth to wavy; the temperature contours are moved alongside the shape of the wall. The heat flow path is almost alike for the wavy wall at aspect ratio up to 0.1 with the smooth hot wall. For δ=0.15, the stem isotherm shifted towards the inclined cold wall and the isotherms with θ≤0.4 are stick with the cold walls.

4.3 Effect of configurations of cold walls

Position AB

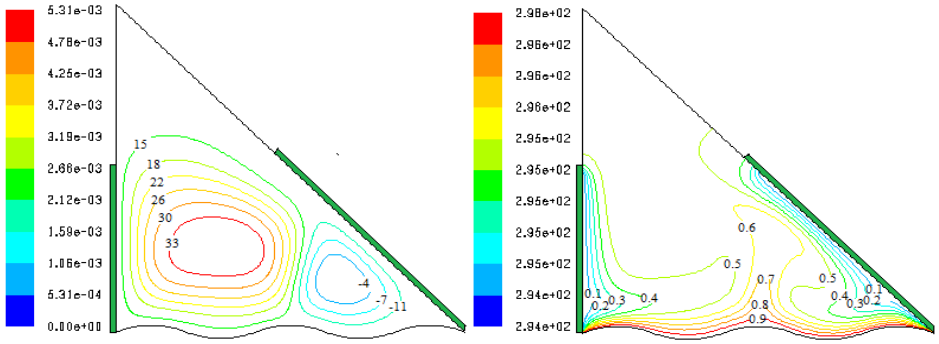

Ψ_{max}=37

Position BC

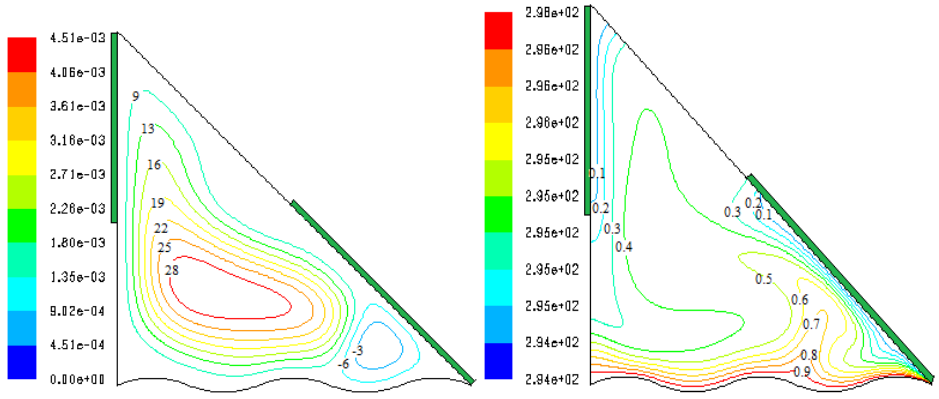

Ψ_{max}=31.3

Position AD

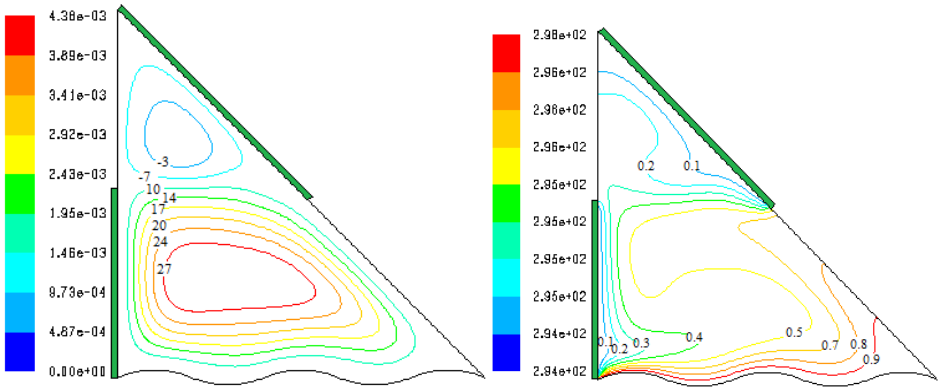

Ψ_{max}=30.4

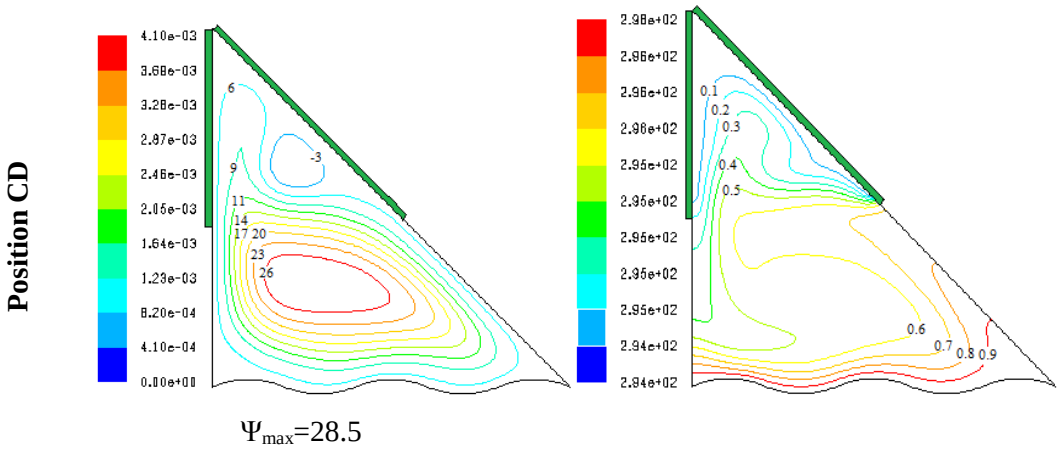

Figure 7: Variation of streamlines (left) and isotherms (right) for different positions of cold walls at δ=0.1and Ra=5×10^5

Fig. 7 illuminates the numerical results to manifest the effect of positions of cold walls on flow behavior and temperature distribution via streamlines (left) and isotherms (right) at δ=0.1 for Ra=5×10^5. Two vortexes of the streamlines are formed in different structures inside the cavity according to the configurations of the cold walls. In first two configurations AB and BC; left side cell is rotated in an anticlockwise and right cell in clockwise. While in the last two cases; lower cell rotates in anticlockwise and the upper one in clockwise. It is significant to stipulate that the strength of anticlockwise rotation is stronger than that of clockwise rotation for all positions of the cold walls as the effect of cold walls configurations dominate over the buoyancy strength. The flow rotational strength decreases gradually as the position is shifted from AB to CD. It happens because the fluids particles have to cover a long path to transmit the heat from hot to cold walls.

The isotherms contours are also getting affected by the configurations of cold walls corresponding to streamlines as shown in right column of Fig. 7. The isotherms are in shape of the base wall adjacent to it. When the cold walls are in AB position, the isotherms contour with θ≤0.5 are compassed through the cavity but clustered near the cold walls. On another hand, these get spanned the entire cavity when the positions of cold walls are changed from AB to BC, AD and CD. The distribution of isotherm inside the whole cavity shows the heat flow. If the cold wall is placed in the flow direction, higher heat transfer rate is occurred because of the closeness of hot and cold walls, if not, heat transfer rate is getting low. That is why the heat transfer rate for cold walls positions AB and BC is higher than AD and CD positions.

4.4 Effect of Rayleigh number

Ra=1×10^5

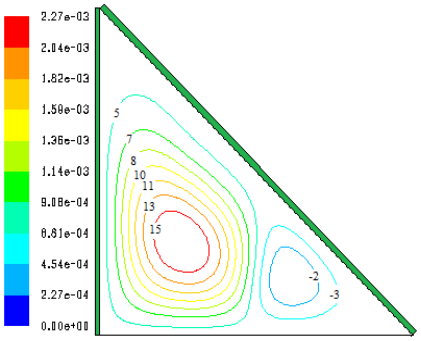

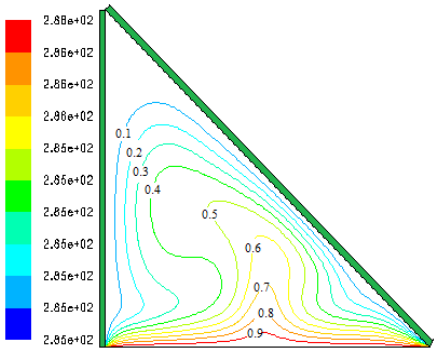

Ψ_{max}=16.3

Ra=5×10^5

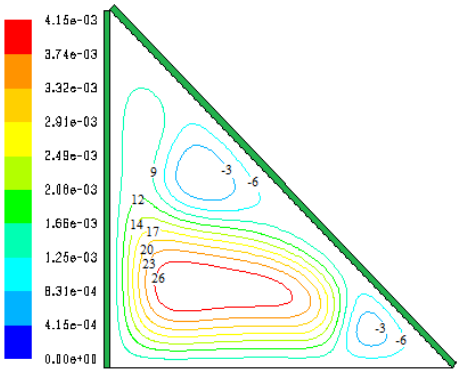

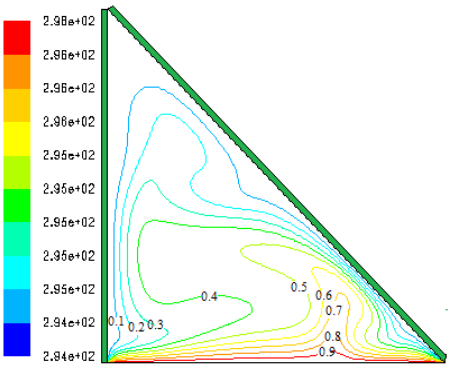

Ψ_{max}=29

Ra=1×10^6

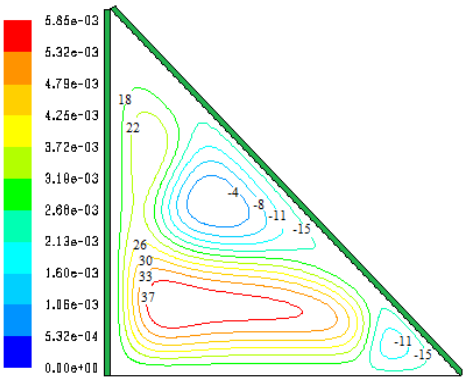

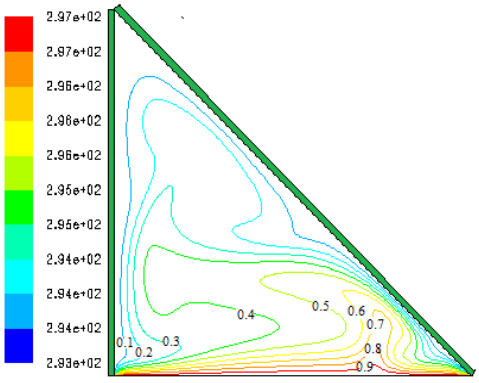

Ψ_{max}=40.6

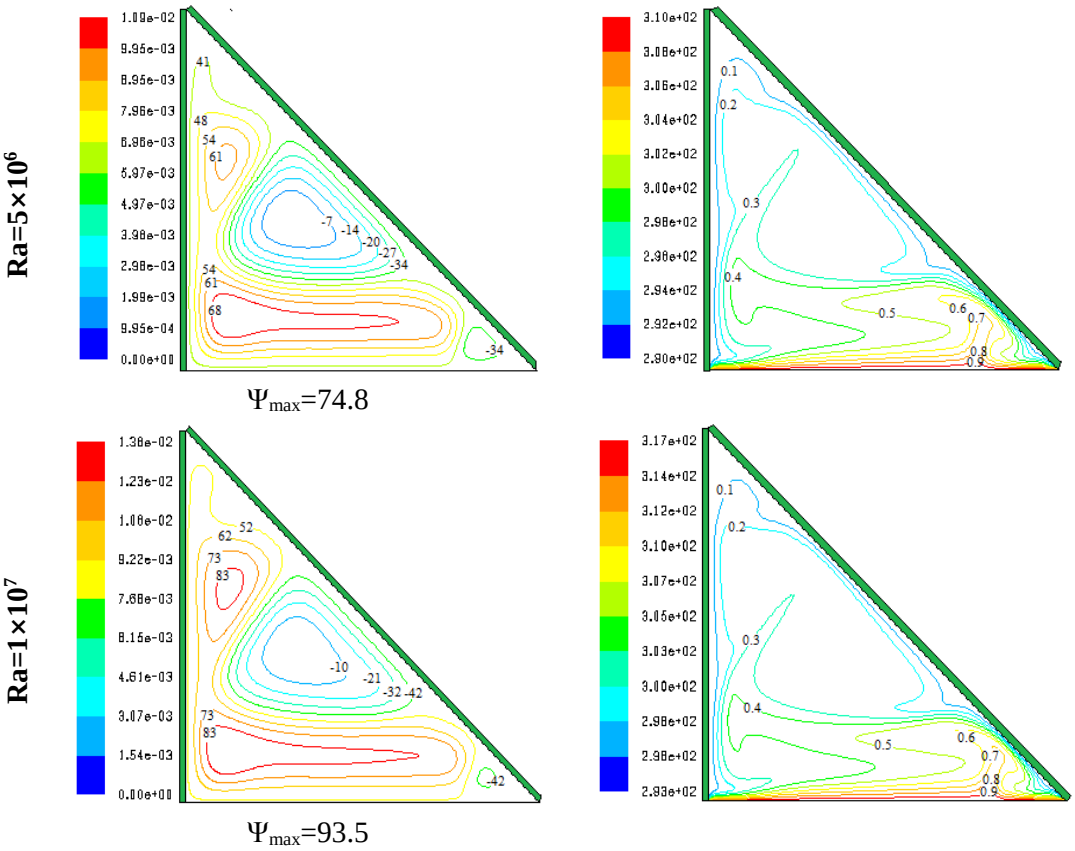

Figure 8: Variation of streamlines (left) and isotherms (right) at different Rayleigh number and δ=0 for the full length of the cold walls

Fig. 8 portrays the influence of different Rayleigh number on streamline and isotherms contours for the full length of cold walls and smooth heating. At Ra=10^5, two asymmetric rotating cells are shaped from the enclosure stem, falling along the side and inclined walls. The streamlines are distorted and shattered into three as the Rayleigh number is increased from 10^5.The magnitude of the stream function is increased as well with the increase of Rayleigh number. Since the temperature gradient is directly related to the Rayleigh number, as a result, the fluid particles absorb heat energy from the source and the buoyancy force gets mounted. Hence, the heat transfer rate is strengthened inside the cavity with the increment of the Rayleigh number. The corresponding contour plots of the isotherms are getting altered with an increase in Rayleigh number. The growth of the thermal boundary layer depends on the temperature gradients between the walls. The lower temperature gradient establishes a weak buoyancy force inside the cavity due to which the isotherms is raised from the middle and not acquired the whole cavity. The intensity of the flow is increased with the increase of Rayleigh number renders the strong buoyancy force which leads to fortify the thermal boundary layer. This strengthens is more significant at the right side of the cavity because of the inclination of the cold wall which brings the hot and cold wall closer and hence the central core of the isotherms with

θ=0.9-0.6 is shifted towards the right corner. However, the contours occupied approximately 95% of the cavity and θ ≤ 0.5 is stick with the cold walls at Ra=10^7.

4.5 Local and average Nusselt number

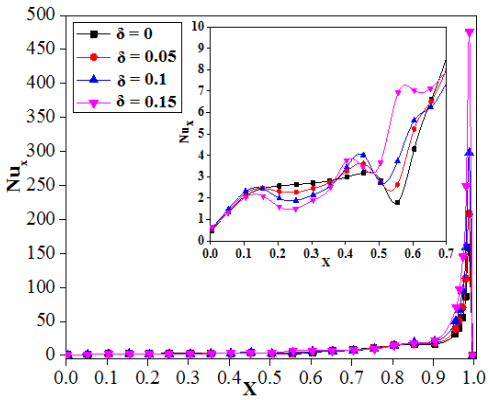

Figure 9: Variation of local Nusselt number with distance for different hot wall aspect ratio at cold wall position AB and Ra=1×10^6

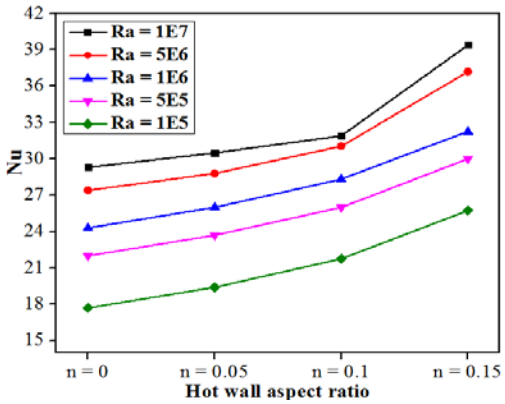

Figure 10: Variation of averageNusselt number with different hot wall aspect ratio for cold wall position AB at different Rayleigh number

Figs. 9 and 10 illuminate the distribution of local and average Nusselt number induced by hot wall aspect ratio. The variation in local Nusselt number is demonstrated for cold wall position AB at Ra=10^6. The sensible increment in local Nusselt number is occurred up to the dimensionless distance 0.1 and it's constantly increasing up to X=0.5. While the Nu_x is escalated at every crest of the curve since it is known that the heat transfer rate is affected by the irregularity of the surface. As the smooth wall is replaced by a sinusoidal wall with varying aspect ratio (0.05-0.15), the surface area of the wall is increased due to which additional numbers of fluid particles come in contact with the wall. The undulations provide ample contact time to the fluid particles with the surface so that they can carry abundant heat from hot to cold walls. It can also be perceived from the average Nusselt number plots which are represented by cold walls position AB at different Rayleigh number. The average Nusselt number plot reveals that the heat transfer rate is enhanced with the increase of undulation aspect ratio. At Ra=10^5, the average Nusselt number, Nu at δ=0.15, 0.1 and 0.5 is 45.4%, 22.9% and 9.6% more than the average number at δ=0, respectively. Although at Ra=10^7, the average Nusselt number, Nu at δ=0.15, 0.1 and 0.5 is 34.5%, 8.9% and 4.1% more than the Nu at δ=0, respectively.

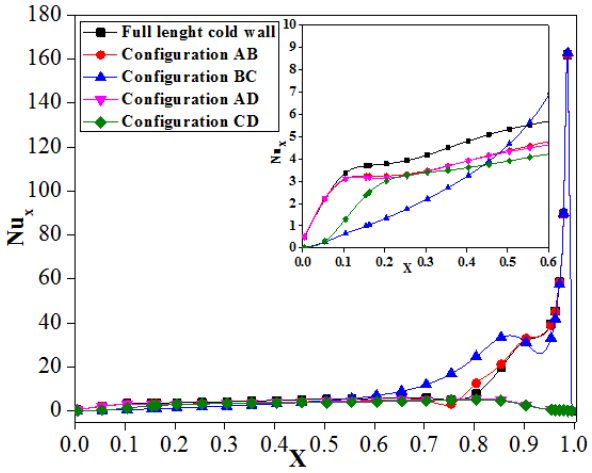

Figure 11: Local Nusselt number distributions with distance for different cold walls configurations at δ=0 and Ra=1×10^7

Fig. 11 demonstrates the distribution of local Nusselt number with distance X for different configurations of cold walls at n=0 and Ra=10^7. The Nusselt number is varied sensibly and constantly up to X=0.6. After that, the abrupt increment in the local Nusselt number is occurred near the right corner of the cavity because of the inclination of the cold wall. This inclination brings the hot and cold wall closer; however some fluid particles get trapped as well at the right corner due to the narrowness. At this part, the transfer of heat is occurred due to conduction while beside of it, convection heat transfer is functioning. Hence, heat flow is found to be high at the right part of the cavity. The higher value of a local Nusselt number is found for the full length of a side, inclined cold walls and partially active cold walls positions AB and BC.

a) **b)**

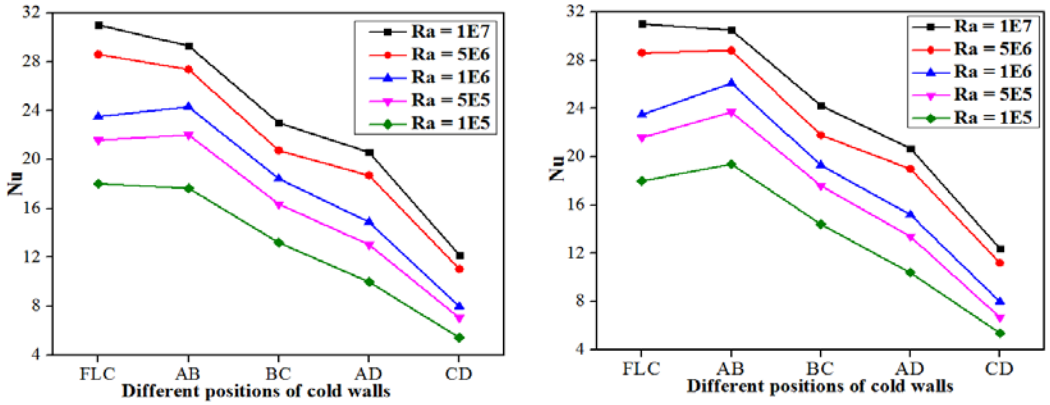

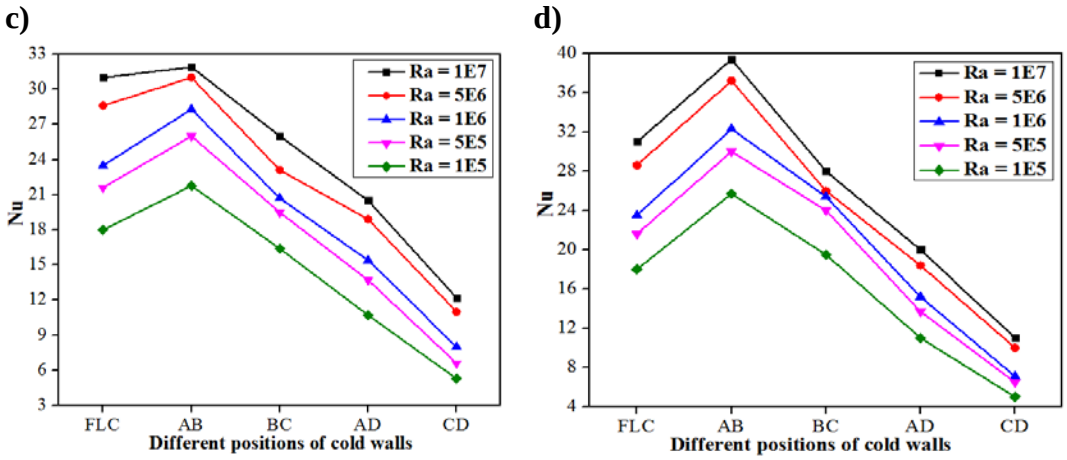

Figure 12: Average Nusselt number variation with different configuration of cold walls for different Rayleigh number at a) δ=0, b) δ=0.05, c) δ=0.1 and d) δ=0.15

The variation in the average Nusselt number with different configurations of cold walls and Rayleigh number at various aspect ratios of the hot wall are exhibited in Fig. 12(a-d). At δ=0, the high heat transfer rate is found for the full-length cold walls at $Ra=10^5$, 5×10^6 and 10^7. However, at $Ra=5\times10^5$ and 1×10^6, the better heat transfer rate is obtained for partially active cold walls configuration AB compared to the full-length cold walls of the cavity. It is interesting to observe that the partially active cold walls are performed excel, especially for AB configuration than the full side and inclined cold walls when the smooth wall is replaced by a sinusoidal wall. The sinusoidal wall with δ=0.05, the average Nusselt number for position AB is higher for all Rayleigh number except at $Ra=10^7$ where the mean Nusselt number is nearly equal with the smooth hot wall. Moreover, the average Nusselt number is higher for position AB at δ=0.1 and δ=0.15 for all Rayleigh number rather than the full length of the side and inclined cold walls. From the plots, it can be stated that the heat transfer rate is significantly remarkable at a higher aspect ratio of the sinusoidal hot wall which is not much effective at lower aspect ratio. Also, the enhancement in the average Nusselt is observed at δ=0.15 for the configuration of cold walls BC. In the case of smooth heating such as at δ=0, the average Nusselt number, Nu_{FLC} is just 2% higher than the Nu_{AB} at $Ra=10^5$ while it is 5.8% at $Ra=10^7$. For sinusoidal heating, at δ=0.05, the Nu_{AB} is 7.8% higher than the Nu_{FLC} at $Ra=10^5$ on the other hand Nu_{FLC} is about 1.8% more than the Nu_{AB} at $Ra=10^7$. The Nu_{AB} is 20.8% higher than Nu_{FLC} for $Ra=10^5$ while it is just 3% at $Ra=10^7$ at n=0.1. At last, at n=0.15, the Nu_{AB} is 42.8% higher than Nu_{FLC} at $Ra=10^5$ as it is 27.1% at $Ra=10^7$. Furthermore, the average Nusselt number for position BC is enhanced up to $Ra=10^6$ compared to the full length of cold walls.

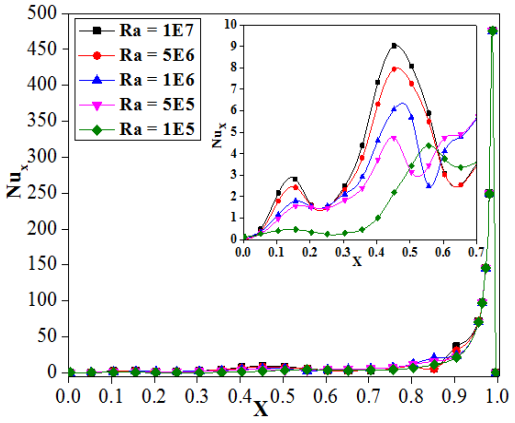

Figure 13: Distributions of local Nusselt number with distance for different Rayleigh number at δ=0.15 and configuration BC

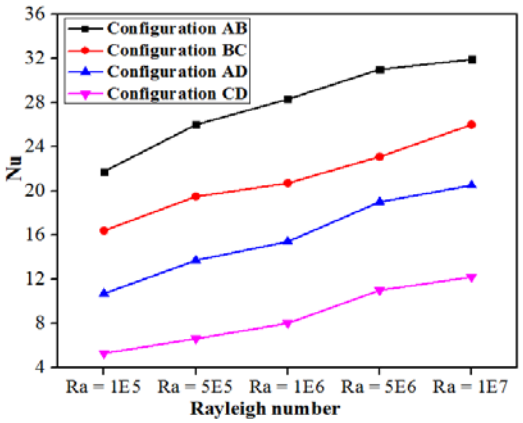

Figure 14: Average Nusselt number variation with Rayleigh number for cold walls positions AB, BC, AD and CD at δ=0.1

Fig. 13 depicts the variation in local Nusselt number at δ=0.15 and cold walls configuration BC for different Rayleigh number. As expected the local Nusselt number is enhanced with the increase of Rayleigh number. It is quite obvious because the heat energy received by the fluid depends on the temperature gradient between the walls which is proportionately related to the values of Rayleigh number. The magnitude of the temperature gradient is smaller at the lower Rayleigh number thus the lesser amount of heat energy received by the fluid is unable to set a strong buoyancy force inside the cavity. As the Rayleigh number is increased the strong buoyancy force is built up inside the cavity which escalated the rotational flow of the fluid. A high convective heat transfer is occurred due to strong buoyancy force which elevated the magnitude of convective heat transfer coefficient and hence the local and average Nusselt numbers are enhanced. These variations can be observed from Figs. 13 and 14. The local Nusselt number is higher at every crest of the sinusoidal curve and it is enhanced with the increase of Rayleigh number. Also, the significant enhancement in average Nusselt number is found for the higher magnitude of Rayleigh number.

5 Conclusion

The current numerical investigation is carried out to examine the natural cooling of the sinusoidal base hot wall with different aspect ratio using partially active cold walls in right triangular cavity for different values of Rayleigh number. The aspect ratio (δ) of the hot wall is varied from 0 to 0.15. The vertical and inclined walls are detached from the middle and arranged in a four different configuration namely AB, BC, AD, and CD for cooling. The cavity has been filled with water and finite volume method is used to discretize the governing equations. The fluid movement and heat flow have been visualized by streamlines and isotherms.

- The rate of heat transfer is presented through local and average Nusselt numbers which are significantly affected by the sinusoidal shape of the hot wall than the

plane wall. However, the hot wall with sinusoidal shape gets exaggerated with partially active cold walls.

- The average Nusselt number, Nu_{FLC} is 5.8% more than the Nu_{AB} at $Ra=10^7$while it is only 2% more at $Ra=10^5$. Nevertheless, there is not much difference in Nu between the full length of cold walls and partially active cold walls with configuration AB. Hence this partial configuration may be used instead of full vertical and inclined cold walls for heating through the plane wall.
- The sinusoidal heating is seemed quite apt with partially cooling than the full length of cold walls. At $\delta=0.05$, the Nu_{AB} is 7.8% higher than Nu_{FLC} at $Ra=10^5$, conversely $Nu_{FLC}$is just 1.8% high than Nu_{AB} at $Ra=10^7$.
- On $\delta=0.1$, the average Nusselt number, Nu_{AB} is 20.8% more than Nu_{FLC} for $Ra=10^5$ while it is now 3% at $Ra=10^7$.
- Finally, at $\delta=0.15$, the Nu_{AB} is 42.8% higher than Nu_{FLC} at $Ra=10^5$ as it is 27.1% more than Nu_{FLC}at $Ra=10^7$. However, the enhancement in average Nusselt number is observed for the configuration BC between the ranges 10^5-10^6 of Rayleigh number. The Nu_{BC} is 8.3% at $Ra=10^5$, it is 11.1% at $Ra=5\times10^5$ and 8.1% more than Nu_{FLC} at $Ra=10^6$.
- It is interesting to encapsulate that the better enhancement in heat transfer rate is observed at lower Rayleigh number rather than higher. So, this scheme (sinusoidal heating with partially active cold walls) may be beneficial for cooling the equipment at lower temperature gradient. However, the average Nusselt number for configurations AD and CD is less compared to the full length of the cold walls for all Rayleigh number; therefore, these configurations may be used as heat transfer rate control parameter.

Reference

Abu-Nada, E.; Masoud, Z.; Oztop, H. F.; Campo, A. (2010): Effect of nanofluid variable properties on natural convection in enclosures. *International Journal of Thermal Sciences*, vol. 49, pp. 479-491.

Akinsete, V. A.; Coleman, T. A. (1982): Heat transfer by steady laminar free convection in triangular enclosures. *International Journal of Heat and Mass Transfer*, vol. 25, pp. 991-998.

Aminossadti, S. M. (2013): Hydromagnetic natural cooling of triangular heat source in a triangular cavity with water-CuO nanofluid. *International Communications in Heat Mass Transfer*, vol. 43, pp. 22-29.

Asan, H.; Namli, L. (2000): Laminar natural convection in a pitched roof of triangular cross-section: summer day boundary conditions. *Energy and Buildings*, vol. 33, pp. 69-73.

Ben Nasr, K.; Chouikh, R.; Kerkeni, C.; Guizani, A. (2006): Numerical study of the natural convection in cavity heated from the lower corner and cooled from the ceiling. *Applied Thermal Engineering*, vol. 26, pp. 772-775.

Bocu, Z.; Altac, Z. (2011): Laminar natural convection heat transfer and air flow in three-dimensional rectangular enclosures with pin arrays attached to hot wall. *Applied Thermal Engineering*, vol. 31, pp. 3189-3195.

Dalal, A.; Das, M. K. (2005): Laminar natural convection in an inclined complicated cavity with spatially variable wall temperature. *International Journal of Heat and Mass Transfer*, vol. 48, pp. 2986-3007.

Flack, R. D.; Konopnicki, T. T.; Rooke, J. H. (1979): The measurement of natural convective heat transfer in triangular enclosures. *Journal of Heat Transfer*, vol. 101, pp. 770-772.

Fluent User's Guide, Release 6.3.26, Fluent Incorporated (2005-01-06).

Ganzarolli, M. M.; Milanez, L. F. (1995): Natural convection in rectangular enclosures heated from below and symmetrically cooled from the sides. *International Journal of Heat Mass Transfer*, vol. 38, pp. 1063-1073.

Nansteel, M. W. (1984): An investigation of natural convection in enclosures with two and three dimensional partitions. *International Journal of Heat Mass Transfer*, vol. 27, pp. 561-571.

Ostrach, S. (1988): Natural convection in enclosures. *Journal of Heat Transfer*, vol. 110, pp. 1175-1190.

Pesso, T.; Piva, S. (2009): Laminar natural convection in a square cavity: Low prandtls numbers and large density differences. *International Journal of Heat and Mass Transfer*, vol. 52, pp. 1036-1043.

Rahimi, M.; Ranjbar, M. J.; Hosseini, M. J. (2012): Natural convection of nanoparticle-water mixture near its density inversion in a rectangular enclosure. *International Communications in Heat Mass Transfer*, vol. 39, pp. 131-137.

Rahman, M. M.; Oztop, H. F.; Ahsan, A.; Orfi, J. (2012): Natural convection effects on heat and mass transfer in a curvilinear triangular cavity. *International Journal of Heat and Mass Transfer*, vol. 55, pp. 6250-6259.

Rahman, M. M.; Saidur, R.; Mekhilef, S.; Uddin, M. B.; Ahsan, A. (2013): Double-diffusive buoyancy induced flow in a triangular cavity with corrugated bottom wall: Effects of geometrical parameters. *International Communications in Heat and Mass Transfer*, vol. 45, vol. 64-74.

Ramakrishn, D.; Basak, T.; Roy, S.; Momoniat, E. (2014): Analysis of thermal efficiency via analysis of heat flow and entropy generation during natural convection within porous trapezoidal cavities. *International Journal of Heat and Mass Transfer*, vol. 77, pp. 98-113.

Triveni, M. K.; Panua, R. S. (2016): Numerical simulation of natural convection in a triangular enclosure with caterpillar (C)-curve shape hot wall. *International Journal of Heat and Mass Transfer*, vol. 96, pp. 535-547.

Triveni, M. K.; Panua, R. S.; Sen, D. (2015): Natural convection in a partially heated triangular cavity with different configurations of cold walls. *Arabian Science for Science and Engineering*, vol. 40, pp. 3285-3297.

Triveni, M. K.; Sen D.; Panua, R. S. (2014): Laminar natural convection for thermally active partial side walls in a right-angled triangular cavity. *Arabian Science for Science and Engineering*, vol. 39, pp. 9025-9038.

Triveni, M. K.; Sen, D.; Panua, R. S. (2016): Numerical study of laminar natural convection in an arch enclosure filled with Al_2O_3-water based nanofluid. *Journal of Applied Fluid Mechanics*, vol. 9, pp. 1927-1936.

Tzeng, S. C.; Liou, J. H.; Jou, R. Y. (2005): Numerical simulation-aided parametric analysis of natural convection in a roof of triangular enclosures. *Heat Transfer Engineering*, vol. 26, pp. 69-79.

Varol, Y.; Oztop, H. F.; Yilmaz, T. (2007): Natural convection in triangular enclosures with protruding isothermal heater. *International Journal of Heat and Mass Transfer*, vol. 50, pp. 2451-2462.

Yesiloz, G.; Aydin, O. (2013): Laminar natural convection in right-angled triangular enclosures heated and cooled on adjacent walls. *International Journal of Heat and Mass Transfer*, vol. 60, pp. 365-374.